J Mater Sci: Mater Electron (2015) 26:7073–7080
DOI 10.1007/s10854-015-3328-1

Synthesis, characterization and optical properties of cobalt and lanthanide doped CdS nanoparticles

Sonika Khajuria[1] · Sumit Sanotra[1] · Jigmet Ladol[1] · Haq Nawaz Sheikh[1]

Received: 30 March 2015 / Accepted: 5 June 2015 / Published online: 12 June 2015

Abstract Cadmium sulphide (CdS) nanoparticles doped with Co^{2+} and co-doped with Co^{2+} and rare earth metallic ions have been prepared by co-precipitation method. The synthesized nanoparticles have been characterized by X-ray powder diffraction studies, energy dispersive X-ray analysis, scanning electron microscopy (SEM), transmission electron microscopy (TEM), UV–visible spectroscopy, particle size by dynamic light scattering and photoluminescence studies. The X-ray diffraction results indicate that CdS nanoparticles can be co-doped with cobalt and rare earth metallic ions without altering XRD pattern. The particle size calculated from XRD results is in range of 40–50 nm. SEM results show that the synthesized particles are spherical in shape and TEM results reveal that synthesized particles have a very small size nearing to Bohr radius for bulk CdS. Absorption spectra of all the samples show strong blue shift from bulk CdS. Interesting luminescence characteristics have been observed for co-doped CdS nanoparticles at room temperature. The relative fluorescence intensity of co-doped samples is significantly higher than that of undoped and Co^{2+} doped CdS nanoparticles.

Electronic supplementary material The online version of this article (doi:10.1007/s10854-015-3328-1) contains supplementary material, which is available to authorized users.

✉ Haq Nawaz Sheikh
hnsheikh@rediffmail.com

[1] Department of Chemistry, University of Jammu, Baba Sahib Ambedkar Road, Jammu Tawi, Jammu 1800 06, India

1 Introduction

Nanomaterials have captured attention of researchers due to their unusual properties arising from their increased surface to volume ratio and changed electronic structure due to quantum confinement [1–3]. The decrease of size due to quantum size effect leads to increase in band gap energy [4] which can be observed by a blue shift of luminescent [5] and absorption spectra [6–8] of nano-sized semiconductors. During the last two decades, nanosized semiconductors stimulated great interest due to their potential applications in diverse areas such as photocatalysis, solar cells, display panels, etc. [9–12]. Cadmium sulphide (CdS) with a wide band gap of 2.4 eV is a very important technological semiconductor material which has been studied for decades.

A considerable interest has been paid to doped nanoparticles with suitable optically active impurities such as transition metal ions and trivalent rare earth ions as it creates new possibilities for property modification and application of nanoparticles [13–20]. These dopant impurities play an important role in changing the electronic structures and transition probabilities of the host material. Doped nanoparticles are expected to offer a new class of nanomaterials with properties different from bulk materials such as high quantum luminescence efficiency [13, 14], high temperature stability [17], long luminescence lifetimes [18] and dopant dependent tunable emission [20]. There have been a few reports on Mn doped CdS with green–yellow–orange luminescence [21] and orange–red luminescence in Cu doped CdS nanoparticles [22, 23]. Recently, Muruganandam et al. [24] have reported the optical, electrochemical and thermal properties of PVP capped Co^{2+} doped CdS nanoparticles.

Simultaneous presence of two kinds of defects known as co-doping is a topic of interest mainly because of the

opportunity to tailor the position and occupancy of the Fermi-energy of the doped semiconductors [25–28]. CdS nanomaterials doped with Li and Eu have been studied in reported literature [29]. Yang et al. [30, 31] reported the synthesis and characterisation of Co and Cu doped ZnS nanocrystallites and also Ni and Mn doped ZnS nanoparticles. In general, luminescence of rare-earth doped systems mainly reflects the properties of the dopant. The electronic structure of rare-earth ions differ from other elements because of incompletely filled $4f^n$ shells. The $4f^n$ electrons are shielded by $5s^2$ and $5p^6$ electron orbitals. Excitation of materials doped with such ions results in sharp line emission due to intra $4f^n$ shell transitions of rare earth ion core [32] which lies in a wide range covering UV, Vis, IR regions of the spectrum.

A relatively large mismatch in radius and charge between RE^{3+} and divalent Cd^{2+} ions is responsible for the unsuccessful incorporation of RE^{3+} into CdS, and hence inefficient energy transfer is often observed. There is little work done on luminescence studies related to semiconductor nanoparticles coactivated with two kind of metallic ions. In the present work we report the synthesis of cobalt and rare earth doped CdS nanoparticles through a simple co-precipitation technique.

For the synthesis of semiconductor nanomaterials, a large number of synthetic methods, like solvo/hydrothermal [33, 34], thermal evaporation [35], plasma method [36], solution based chemical methods [37] and sonochemical method [38–40] have been employed. Co-precipitation method is most popular technique that is used in industrial applications because of the cheap raw materials, easy handling and large scale production [41]. It has been proved one of the useful, simple and fast methods for the synthesis as well as doping of nanostructures.

2 Experimental procedures

2.1 Materials and characterization techniques

All the reagents used were of analytical grade and were used without further purification. Cadmium acetate dihydrate and thioacetamide (TAA) were purchased from Sigma Aldrich. Cobalt(II) chloride hexahydrate ($CoCl_2 \cdot 6H_2O$) was purchased from Thomas Baker and rare earth metal salts, gadolinium(III) chloride hydrate ($GdCl_3 \cdot H_2O$), terbium(III) chloride hexahydrate ($TbCl_3 \cdot 6H_2O$) and erbium(III) chloride hexahydrate ($ErCl_3 \cdot 6H_2O$) were purchased from Sigma Aldrich. Doubly-distilled water was used for preparing aqueous solutions. Powder X-ray diffraction (PXRD) patterns were recorded from 10° to 80° on a Rigaku Miniflex diffractometer using monochromatic CuKα radiations (The Woodlands, TX, USA). Scanning electron micrographs (SEM) were collected on Jeol T-300 scanning electron microscope with gold coating (Tokyo, Japan). Transmission electron micrographs (TEM) were collected on TECNAI 200 Kv TEM (Fei, Electron Optics). The UV–visible (UV) absorption spectra of the samples were recorded on T90+ UV/Vis Spectrophotometer (PG instruments Ltd). The particle size of each compound was determined by dynamic light scattering (DLS) technique using Zetasizer Nano ZS-90 (Malvern Instruments Ltd., Worcestershire, UK). The photoluminescence (PL) excitation and emission spectra were recorded at room temperature using Agilent Cary Eclipse Fluorescence Spectrophotometer equipped with a Xenon lamp that was used as an excitation source.

2.2 Synthesis of Un-doped and doped CdS nanoparticles

The pure/undoped CdS, CdS doped with Co^{2+} and co-doped with Co^{2+}–Gd^{3+}, Co^{2+}–Er^{3+}, Co^{2+}–Tb^{3+} nanoparticles were synthesized in deionized water in an air atmosphere by using chemical precipitation method. The precipitation of various CdS nanoparticles was performed starting with 0.1 M homogeneous solutions of $Cd(CH_3COO)_2 \cdot 2H_2O$ (0.66 g), thioacetamide, TAA, (0.188 g), $CoCl_2 \cdot 6H_2O$ (0.59 g), $GdCl_3 \cdot H_2O$ (0.658 g), $ErCl_3 \cdot 6H_2O$ (0.954 g), $TbCl_3 \cdot 6H_2O$ (0.932 g) each in 25 mL of distilled water. The temperature of each solution was maintained 80 °C and pH was kept at 2 to avoid the decomposition of TAA at premature stage. For the synthesis of pure CdS nanoparticles, aqueous solution of TAA was added dropwise to the solution of $Cd(CH_3COO)_2 \cdot 2H_2O$ while stirring over magnetic stirrer. The reaction temperature was maintained at 80 °C throughout. Stirring was done for 5 h at constant temperature and reaction was terminated by rapidly cooling the reaction mixture in an ice bath. As precipitated doped samples were then centrifuged at 3000 rpm, washed with water and isopropyl alcohol several times and then dried at 70 °C for 2 h. In order to synthesize, Co^{2+} doped CdS nanoparticles, 0.1 M aqueous solutions of $Cd(CH_3COO)_2 \cdot 2H_2O$ (0.66 g) and $CoCl_2 \cdot 6H_2O$ (0.59 g) were mixed and stirred for 30 min. To this, 0.1 M solution of TAA was added dropwise while stirring with reaction temperature maintained at 80 °C. All reaction conditions and procedure adopted were same as above. In a typical synthesis for Co^{2+} and rare earth metallic ions co-doped CdS nanoparticles, 0.1 M aqueous solutions of $Cd(CH_3COO)_2 \cdot 2H_2O$, $CoCl_2 \cdot 6H_2O$ and rare earth metallic ions were mixed and stirred for 30 min. To this mixture, 0.1 M solution of TAA was added dropwise while stirring with reaction temperature maintained at 80 °C. Rest of procedure and reaction conditions were kept similar as for above synthesized nanoparticles.

3 Results and discussion

3.1 XRD measurements

Figure 1 shows XRD patterns of various doped samples. All particles produce highly intense X-ray reflections in their corresponding X-ray powder diffraction (XRPD) pattern indicating that all the compounds are crystalline in nature. The results indicate that particles exhibit hexagonal structure. The six diffraction peaks corresponding to (100), (002), (101), (102), (110), (103) and (112) planes, are indexable to hexagonal phase of CdS (JCPDS 41-1049). No impurity peaks were detected, indicating high purity product. The pattern remains same for all individual doped samples, indicating that hexagonal structure is not altered by addition of different rare earth metals into the matrix at least up to the detection level of XRD. The full width at half maxima of the diffraction peaks were slightly changed by the doping ions. This may be due to a small variation in the particle size. The experimental d-values are in conformity with the obtained calculated ones. Various parameters such as interplanar spacing (d in Å), crystallite size (D in nm), microstrain (ε), dislocation density (ρ in 10^{15} m/m^3) and distortion parameter (g) along (002) plane were calculated using following well known equations and are shown in Table 1. The various equations used are,

$$D = 0.9\lambda/\beta\cos\theta;\ d = \lambda/2\sin\theta;\ \varepsilon = \beta\cos\theta/4;\ \rho = 1/D^2 \text{ and } g = \beta/\tan\beta$$

where $\lambda = 1.5418$ Å for Cu-Kα, β is full width at half maximum (FWHM) of diffraction peaks and θ is diffraction angle. The average crystallite size is found in range of 40–50 nm. The interaction between the dopants and surface/grain boundaries may vary surface energy/grain boundary energy, thus leading the stabilization of the surfaces/grain boundaries and a variation in particle size. Doping makes distortion in the host lattice. Dislocations are generated in order to minimize the sum of the strain and dislocation energies for a given lattice mismatch. The basal dislocations are very mobile and hence the change in stress and strain on doping leads them to move and to regroup to accommodate the changes which results in variation in their values. It is clear from the table that microstrain values decreases with increase in the crystallite size [42].

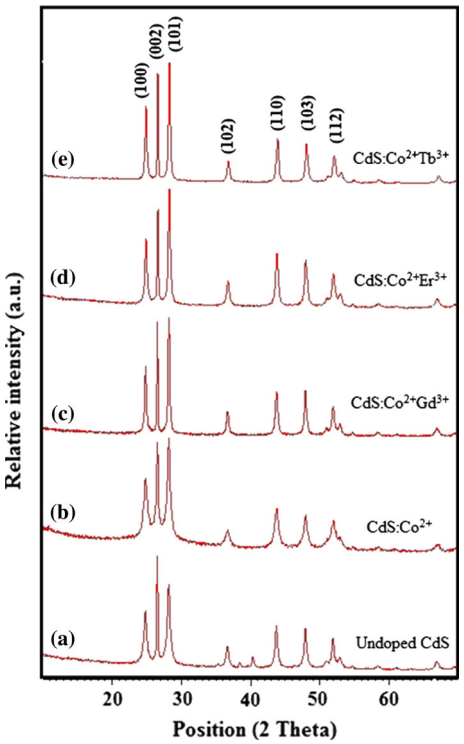

Fig. 1 XRPD patterns for (*a*) undoped CdS, (*b*) CdS:Co^{2+}, (*c*) CdS:Co^{2+} Gd^{3+}, (*d*) CdS:Co^{2+} Er^{3+}, (*e*) CdS:Co^{2+} Tb^{3+} nanoparticles

3.2 EDAX analysis

Energy dispersive X-ray analysis (EDAX) was performed to investigate the presence and concentration of dopant in the doped CdS nanoparticles. Figure 2a–e shows the energy dispersive spectra of the pure, Co^{2+} doped and Co^{2+}, RE co-doped CdS nanoparticles. It has been found that elements cadmium, sulphur, cobalt, gadolinium, erbium, terbium are there in the respective synthesized samples. These results confirm the doping in the CdS nanoparticles. Elemental mapping diagrams show uniform distribution of dopants in all doped samples (See Supplementary Figures S1–S5). There is no impurity phase detected in the EDAX spectra showing the formation of pure phase product.

3.3 SEM and TEM analysis

The morphology and topography of the doped samples was studied using imaging techniques such as scanning electron microscopy (SEM) and transmission electron microscopy (TEM). Figure 3a–e shows SEM images of synthesized undoped, Co^{2+} doped and Co^{2+} and RE^{3+} co-doped nanoparticles. It is evident from the SEM images that synthesized particles have well defined spherical morphology and do not show any aggregation of particles. SEM images also indicate that surface morphology of nanoparticles changes with nature of dopant. Figure 4a–e shows high resolution TEM images of as synthesized nanoparticles. As evident from figure, the particle size of synthesized nanoparticles is very small and falls in the

Table 1 Evaluated parameters from XRPD data for undoped and doped CdS nanoparticles

Samples	Peak position 2θ (degree)	Particle size D (in nm)	FWHM β (in degrees)	d-value (Å)		Micro-strain ε (10^{-3})	Dislocation density ρ (in 10^{15} m/m^3)	Distortion parameter g
				Observed	Calculated			
Undoped CdS	26.67	40.22	0.2007	3.342	3.340	0.710	0.429	0.332
CdS:Co^{2+}	26.73	48.26	0.1673	3.335	3.333	0.852	0.618	0.399
CdS:$Co^{2+}Gd^{3+}$	26.71	60.35	0.1338	3.335	3.336	0.568	0.275	0.266
CdS:$Co^{2+}Er^{3+}$	26.82	48.27	0.1673	3.323	3.322	0.710	0.429	0.330
CdS:$Co^{2+}Tb^{3+}$	26.70	53.60	0.1506	3.338	3.336	0.639	0.348	0.299

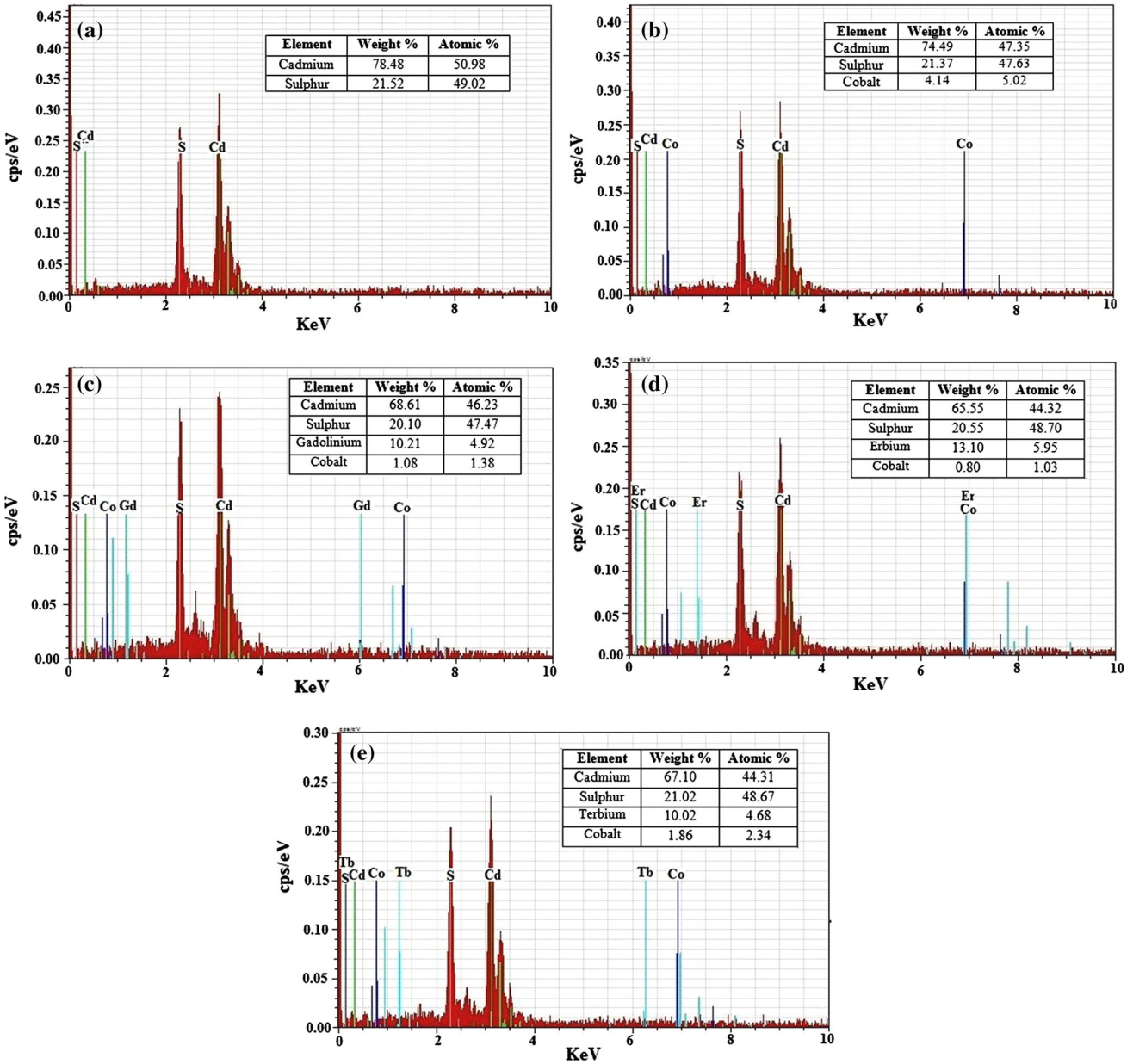

Fig. 2 EDAX spectra for **a** undoped CdS, **b** CdS:Co^{2+}, **c** CdS:Co^{2+} Gd^{3+}, **d** CdS:Co^{2+} Er^{3+}, **e** CdS:Co^{2+} Tb^{3+} nanoparticles

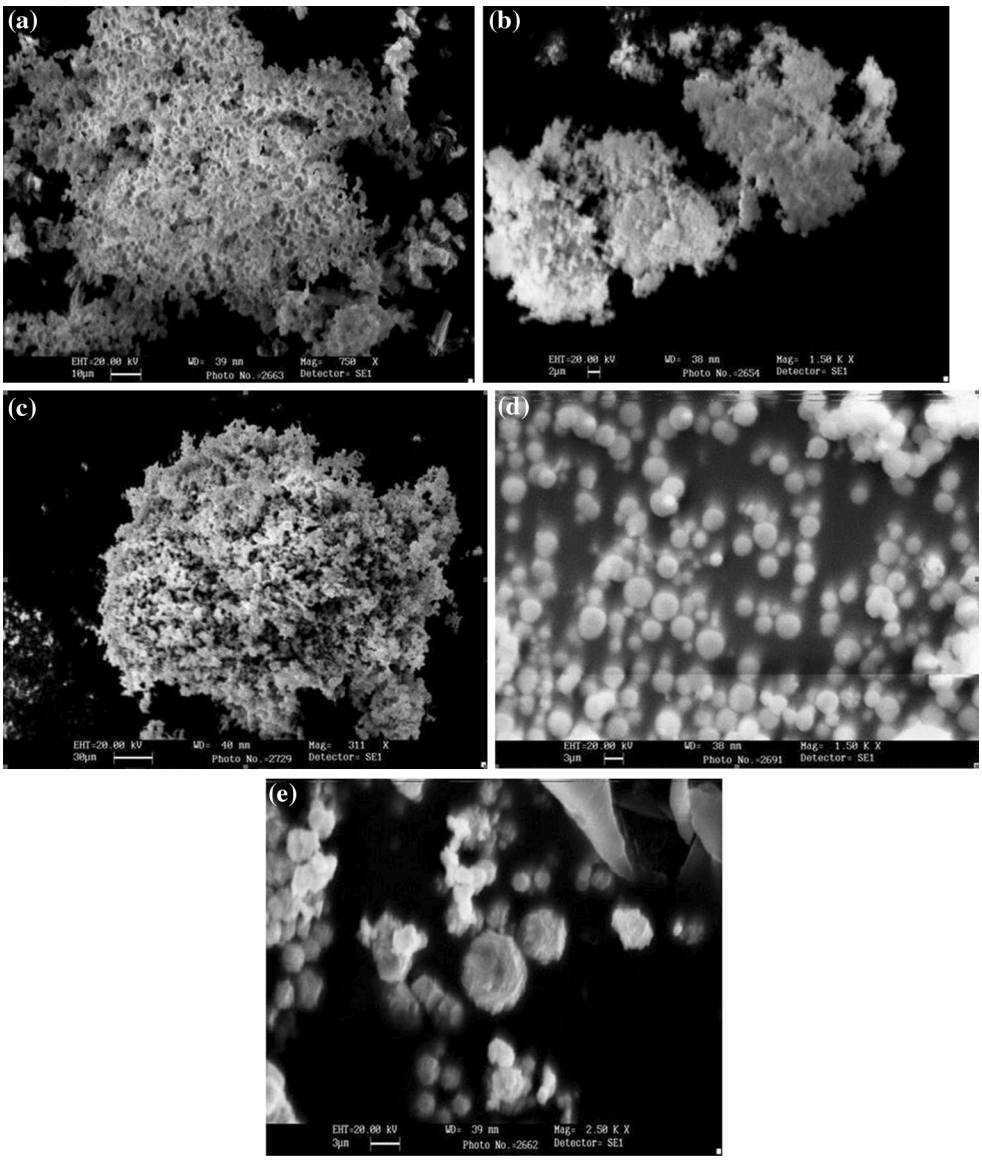

Fig. 3 SEM images for **a** undoped CdS, **b** CdS:Co^{2+}, **c** CdS:Co^{2+} Gd^{3+}, **d** CdS:Co^{2+} Er^{3+}, **e** CdS:Co^{2+} Tb^{3+} nanoparticles

range of the Bohr radius for CdS (about 3 nm). This decrease in size of synthesized nanoparticles is responsible for strong quantum confinement effect and results in interesting properties of synthesized nanoparticles.

3.4 Particle size by dynamic light scattering

Dynamic light scattering technique was used to study particle size distribution of synthesized CdS nanoparticles. The average particle size distribution of all the synthesized samples is presented in Fig. 5. The nanoparticles were uniformly dispersed in isopropyl alcohol by mild sonication for 10 min before DLS analysis. As observed from figure, the approximate sizes of un-doped and doped CdS nanoparticles are different and are found in range of 40–80 nm. The particle size for doped nanoparticls is larger in comparison to undoped one. The particle size analyzed from DLS method is usually larger in comparison to the particle sizes calculated from XRPD data. This is due to surface solvation and agglomeration of particles in colloidal solution. Another reason behind this anomaly is that DLS size measurements assume the spherical shape of the object irrespective of their actual morphology.

3.5 Absorption spectra

The absorption spectra of un-doped CdS, CdS:Co^{2+} doped and CdS:Co^{2+}, RE co-doped nanoparticles are shown in Fig. 6. For recording absorption spectra of samples, as-prepared nanoparticles were dispersed in isopropyl alcohol

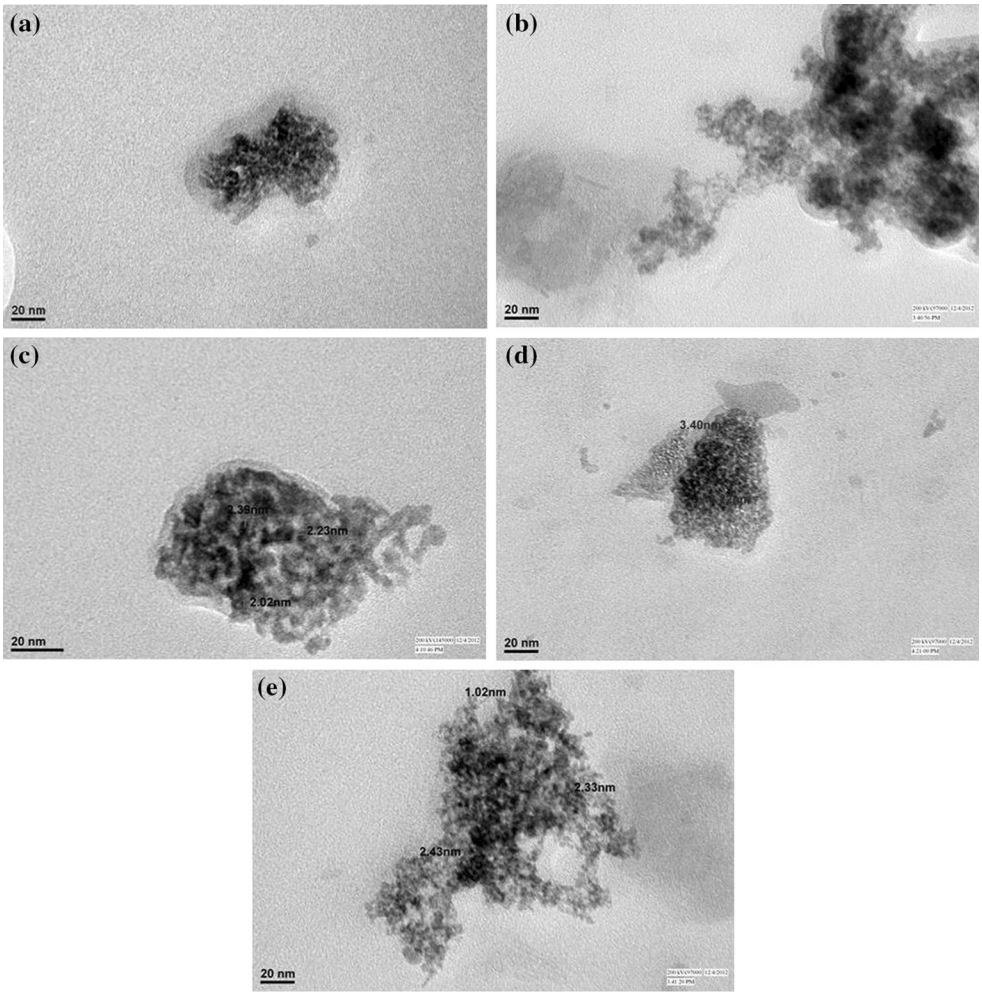

Fig. 4 HRTEM images for **a** undoped CdS, **b** CdS:Co^{2+}, **c** CdS:Co^{2+} Gd^{3+}, **d** CdS:Co^{2+} Er^{3+}, **e** CdS:Co^{2+} Tb^{3+} nanoparticles

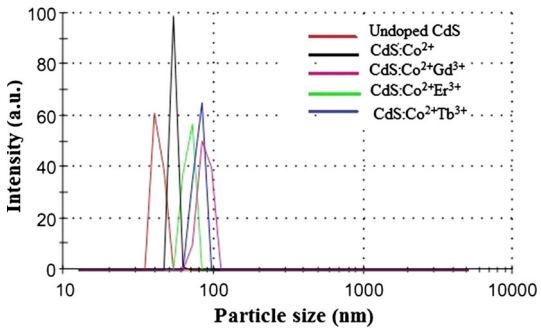

Fig. 5 Particle size by DLS for undoped CdS, CdS:Co^{2+} and CdS:Co^{2+} RE nanoparticles

by ultrasonic washing for about 30 min to obtain nearly monodispersed solutions. All the peaks are strongly blue shifted with respect to the band gap of 515 nm (2.41 eV) for bulk CdS [43]. This blue shift of absorption edge

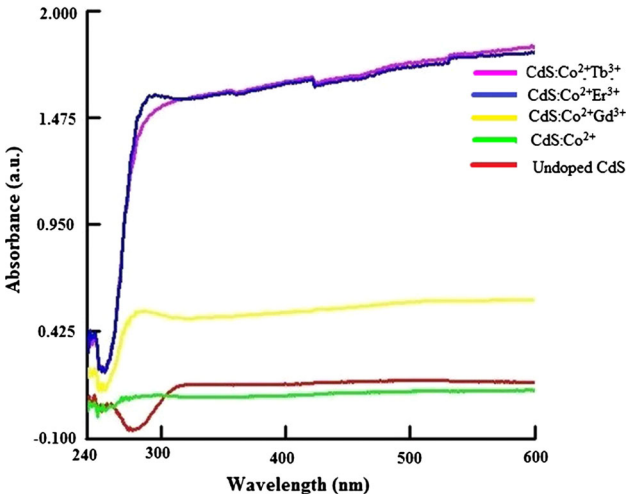

Fig. 6 Absorption Spectra for undoped CdS, CdS:Co^{2+} and CdS:Co^{2+} RE nanoparticles

indicates effect of quantum size confinement in nanoscale materials [44]. This shift occurs because with decreasing size, binding energy of exciton increases due to the increasing columbic overlap enforced by spatial localization of the wave functions. Thambidurai et al. [45] have studied the strong quantum confinement effect in nanocrystalline CdS. Gupta et al. have reported blue shift in the absorbance spectra of Mn^{2+} doped CdS nanoparticles due to strong quantum confinement effect caused by decrease in particle size. For different concentration of dopant (Mn^{2+}), sharp peaks in the range of 234–238 nm were observed [46]. Chawla et al. [47] have also observed such an excitonic peak at 230 nm. Moreover, absorption spectra of doped samples are different from that of un-doped sample. A significant increase in absorption has been observed for Co^{2+}, RE co-doped CdS nanoparticles. However, variation in absorption intensity has been observed with change in the rare earth metal ion as dopant. Also, the absorption peaks for co-doped samples show blue shift as compared to undoped and Co^{2+} doped CdS nanoparticles. Because doped ions can affect the band gap structure of the host materials, the absorption shoulder edge and absorption peak are found to vary with change in the dopant ion.

3.6 Photoluminescence studies

Figure 7 shows PL spectra of un-doped CdS, CdS:Co^{2+} doped and CdS:Co^{2+}, RE co-doped nanoparticles normalized with respect to spectrum of CdS:Co^{2+}, Er^{3+} co-doped sample showing highest intensity. The photoluminescent intensities for nanoscale particles are higher than those of bulk material as they have higher surface/volume ratio and more surface states and thus contain more accessible carriers for PL [48]. We have investigated the effect of doping on the emission of synthesized CdS nanoparticles. The peak position in all the PL spectra is nearly same. However, intensity is significantly changed. A strong emission band centred at about 537 nm along with a weak emission around 575 nm is observed for all the synthesized (un-doped and doped) samples at an excitation of 260 nm. A very small decrease in intensity is observed for CdS:Co^{2+} doped nanoparticles but for CdS:Co^{2+}, RE co-doped nanoparticles, intensity is remarkably enhanced in comparison to un-doped CdS nanoparticles. Strong photoluminescent emission is due to increased recombination of electrons trapped inside a sulphur vacancy with holes in the valance band. In case of CdS nanoparticles codoped with Co^{2+} and RE ions, the composite luminescence centres are formed. On absorption of ultraviolet photons by the nanosized CdS matrix, the electrons are excited from the valence band to the conduction band and are trapped by the defects. Recombination of defects and excited states induced by the composite centre of Co^{2+} and RE ions occurs and visible light emission is observed. When Co^{2+} and RE are doped as activation ions in CdS nanoparticles, more electrons are easily excited and radiative recombination of luminescence process is enhanced. Thus, relative luminescence intensity of co-doped samples is dramatically enhanced. Muruganandam et al. [24] have reported green emission for Co^{2+} doped CdS nanoparticles with emission bands centred at about 529 and 547 nm. Rajesh Kumar et al. [49] reported a strong emission peak at 535 nm with a weak green emission peak at 575 nm for Mn doped CdS nanoparticles capped with PVP. In general, purity in color of substance can be recognized by means of color coordinates. Hence, in our present work, the chromaticity coordinates of CdS nanoparticles have been calculated from the emission spectrum by using the commission international De I'Eclairage (CIE) system. The CIE chromaticity diagram for CdS nanoparticles upon excitation at 260 nm is

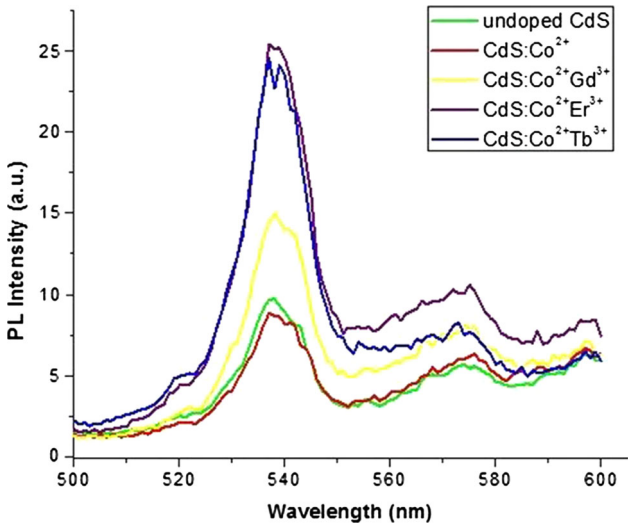

Fig. 7 Photoluminescence spectra for undoped CdS, CdS:Co^{2+} and CdS:Co^{2+} RE nanoparticles

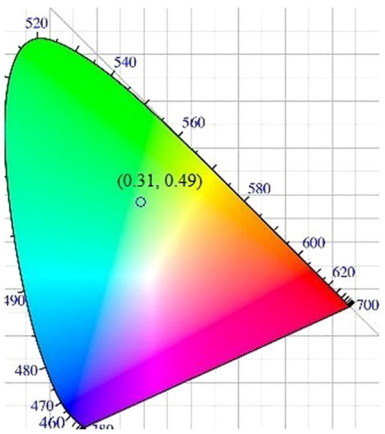

Fig. 8 CIE chromatogram for CdS nanoparticles (Color figure online)

shown in Fig. 8. The CIE coordinate is (0.31, 0.49) which lies within the green region. Therefore, it may be concluded that synthesized nanoparticles can serve as a green color producing material for display applications and light emitting diodes.

4 Conclusions

The CdS nanoparticles doped with Co^{2+} and co-doped with Co^{2+}–Gd^{3+}, Co^{2+}–Er^{3+}, Co^{2+}–Tb^{3+} were obtained by co-precipitation method. XRPD results suggest that co-doping does not alter the XRD pattern of CdS nanoparticles. Optical absorption of all the samples was fairly blue shifted compared to bulk CdS due to quantum confinement effect. PL experiments show very strong visible light emission from co-doped nanoparticles at room temperature. The emission peak of un-doped CdS is centered at about 537 nm. Although the peak position of doped and co-doped CdS nanopaticles is at the same position but their fluorescence intensities are remarkably enhanced compared to un-doped CdS nanoparticles.

Acknowledgments We gratefully acknowledge Sophisticated Analytical Instrumentation Facility, Panjab University, Chandigarh for powder X-ray diffraction study. We thank, All India Institute of Medical Sciences (AIIMS), New Delhi for transmission electron microscopy. The authors thank Dr. Vinay Kumar, Assistant Professor, School of Physics, Shri Mata Vaishno Devi University (SMVDU) for photoluminescence studies.

References

1. M.M. Kholoud, A. El-Nour, A. Eftaiha, A. Al-Warthan, R.A.A. Ammar, Arab. J. Chem. **3**, 135 (2010)
2. B. Dong, L. Cao, G. Su, W. Liu, H. Qu, H. Zhai, J. Alloys Compd. **492**, 363 (2010)
3. X.J. Zheng, Y.Q. Chen, T. Zhang, B. Yang, C.B. Jiang, B. Yuan, Z. Zhu, Sens. Actuators B Chem. **147**, 442 (2010)
4. Y. Wang, N. Herron, J. Phys. Chem. **95**, 525 (1991)
5. G. Murugadoss, Spectrochim. Acta A **93**, 53 (2012)
6. N. Tit, M.W.C. Dharma-Wardana, Solid State Commun. **106**, 121 (1998)
7. Z.L. Wang, Y. Liu, Z. Zhang, *Handbook of Nanophase and Nanostructured Materials—Characterization* (Tsinghua University Press and Kluwer, 2002)
8. A. Cortes, H. Gomez, R.E. Marotti, G. Riveros, E.A. Dalchiele, Sol. Energy Mater. Sol. Cells **82**, 21 (2004)
9. G.Y. Ni, J. Yin, Z.X. Hong, Mater. Res. Bull. **39**, 1967 (2004)
10. D. Moore, C. Ronning, C.M. Zhong, L. Wang, Chem. Phys. Lett. **385**, 8 (2004)
11. P. Roy, J.R. Ota, S.K. Srivastava, Thin Solid Films **515**, 1912 (2006)
12. S. Lee, D. Song, D. Kim, J. Lee, S. Kim, J.Y. Paric, Y.D. Choi, Mater. Lett. **58**, 342 (2004)
13. R.N. Bhargava, D. Gallagher, X. Hong, A. Nurmikko, Phys. Rev. Lett. **72**, 416 (1994)
14. R. Reisfeld, M. Gaft, T. Saridarov, G. Panczer, M. Zelner, Mater. Lett. **45**, 154 (2000)
15. F.V. Mikulec, M. Kuno, M. Bennati, D.A. Hall, R.G. Griffin, M.G. Bawendi, J. Am. Chem. Soc. **122**, 2532 (2000)
16. O.E. Raola, G.F. Strouse, Nano Lett. **2**, 1443 (2002)
17. R.S. Zeng, M. Rutherford, R.G. Xie, B.S. Zou, X.G. Peng, Chem. Mater. **22**, 2107 (2010)
18. D.A. Chengelis, A.M. Yingling, P.D. Badger, C.M. Shade, S. Petoud, J. Am. Chem. Soc. **127**, 16752 (2005)
19. R. Viswanatha, D.M. Battaglia, M.E. Curtis, T.D. Mishima, M.B. Johnson, X.G. Peng, Nano Res. **1**, 138 (2008)
20. W.Z. Wu, H.A. Ye, X.L. Ruan, Nanotechnology **21**, 265704 (2010)
21. A. Ishizumi, K. Matsuda, T. Saiki, C.W. White, Y. Kanemitsu, Appl. Phys. Lett. **87**, 133104 (2005)
22. H. Kato, J. Sato, T. Abe, Y. Kashiwaba, Phys. Status Solidi C **1**, 653 (2004)
23. V. Ghiordanescu, M. Sima, I. Enculescu, M.N. Grecu, R. Neumann, Phys. Status Solidi A **202**, 449 (2005)
24. S. Muruganandam, G. Anbalagan, G. Murugadoss, Appl. Nanosci. **5**, 245 (2015)
25. M.J. Reed, F.E. Arkun, E.A. Berkman, N.A. Elmasry, J. Zavada, M.O. Luen, M.L. Reed, S.M. Bedair, Appl. Phys. Lett. **86**, 102504 (2005)
26. S. Kuroda, N. Nishizawa, K. Takita, M. Mitome, Y. Bando, K. Osuch, T. Dietl, Nat. Mater. **6**, 440 (2006)
27. M.H. Kane, M. Strassburg, W.E. Fenwick, A. Asghar, A.M. Payne, S. Gupta, Q. Song, Z.J. Zhang, N. Dietz, C.J. Summers, I.T. Ferguson, J. Cryst. Growth **287**, 591 (2006)
28. N. Ozaki, I. Okabayashi, T. Kumekawa, N. Nishizawa, S. Marcet, S. Kuroda, K. Takita, Appl. Phys. Lett. **87**, 192116 (2005)
29. N.S. Gajbhiye, R.S. Ningthoujam, A. Ahmed, D.K. Panda, S.S. Umare, S.J. Sharma, Pramana-J. Phys. **70**, 313 (2008)
30. P. Yang, M. Lu, G. Zhou, D.R. Yuan, D. Xu, Inorg. Chem. Commun. **4**, 734 (2001)
31. P. Yang, M. Lu, D. Xu, D. Yuan, C. Song, S. Liu, X. Cheng, Opt. Mater. **24**, 497 (2003)
32. H.J. Lozykowski, W.M. Jadwisienkzak, I. Brown, J. Appl. Phys. **88**, 210 (2000)
33. J.S. Jang, U.A. Joshi, J.S. Lee, J. Phys. Chem. C **111**, 13280 (2007)
34. F. Chen, R.J. Zhou, L.G. Yang, M.M. Shi, G. Wu, M. Wang, H.Z. Chen, J. Phys. Chem. C **112**, 13457 (2008)
35. S. Kar, S. Chaudhuri, J. Phys. Chem. B **110**, 4542 (2006)
36. U. Kortshagen, L. Mangolini, A. Bapat, J. Nanopart. Res. **9**, 39 (2007)
37. R.J. Bandaranayake, G.W. Wen, J.Y. Lin, H.X. Jiang, C.M. Sorensen, Appl. Phys. Lett. **67**, 831 (1995)
38. J.H. Bang, K.S. Suslick, Adv. Mater. **22**, 1039 (2010)
39. A. Khataee, A. Karimi, S.A. Oskoui, R.D.C. Soltani, Y. Hanifehpour, B. Soltani, S.W. Joo, Ultrason. Sonochem. **22**, 371 (2015)
40. Z.H. Hafeezullah, J. Yamani, A. Iqbal, A.Hakeem Qurashi, J. Alloys Compd. **616**, 76 (2014)
41. A.H. Souici, N. Keghouche, J.A. Delaire, H. Remita, M. Mostafavi, Chem. Phys. Lett. **422**, 25 (2006)
42. A.L. Dawer, P.K. Shishodia, J. Chouhan, G. Kumar, A. Mathur, Mater. Sci. Lett. **9**, 547 (1990)
43. P.S. Nair, N. Revaprasadu, T. Radhakrishnana, G.A. Kolawolea, J. Mater. Chem. **11**, 1555 (2001)
44. J. Nanda, S. Sapra, D.D. Srama, N. Chandrasekharan, G. Hodes, Chem. Mater. **12**, 1018 (2000)
45. M. Thambidurai, N. Muthukumarasamy, S. Agilan, N. Murugan, S. Vasantha, R. Balasundaraprabhu, T.S. Senthil, J. Mater. Sci. **45**, 3254 (2010)
46. A.K. Gupta, R. Kripal, Spectrochim. Acta A **96**, 626 (2012)
47. P. Chawla, G. Sharma, S.P. Lochab, N. Singh, Radiat. Eff. Defect. S. **164**, 755 (2009)
48. W. Chen, Z.G. Wang, Z.J. Lin, L.Y. Lin, Appl. Phys. Lett. **70**, 1466 (1997)
49. M.R. Kumar, G. Murugadoss, J. Lumin. **146**, 325 (2014)